




# A comprehensive study on the optical, mechanical, and radiation shielding properties of the $\text{TeO}_2\text{--Li}_2\text{O--GeO}_2$ glass system

Norah A. M. Alsaif<sup>1</sup>, Mohammed Alotiby<sup>2</sup>, M. Y. Hanfi<sup>3,4,\*</sup> , M. I. Sayyed<sup>5,6</sup>, K. A. Mahmoud<sup>3,4</sup>, B. M. Alotaibi<sup>1</sup>, Haifa A. Alyousef<sup>1</sup>, and Y. Al-Hadeethi<sup>7</sup>

<sup>1</sup>Department of Physics, Faculty of Science, Princess Nourah bint Abdulrahman University, Riyadh, Saudi Arabia

<sup>2</sup>King Abdulaziz City for Science and Technology, Riyadh, Saudi Arabia

<sup>3</sup>Ural Federal University, St. Mira, 19, 620002 Yekaterinburg, Russia

<sup>4</sup>Nuclear Materials Authority, Maadi, Cairo, Egypt

<sup>5</sup>Department of Physics, Faculty of Science, Isra University, Amman 11622, Jordan

<sup>6</sup>Department of Nuclear Medicine Research, Institute for Research and Medical Consultations, Imam Abdulrahman Bin Faisal University, Dammam 31441, Saudi Arabia

<sup>7</sup>Department of Physics, Faculty of Science, King Abdulaziz University, Jeddah 21589, Saudi Arabia

Received: 27 February 2021

Accepted: 26 April 2021

Published online:

11 May 2021

© The Author(s), under exclusive licence to Springer Science+Business Media, LLC, part of Springer Nature 2021

## ABSTRACT

This paper summarized a comprehensive study on mechanical, optical, and shielding features of the binary lithium-tellurite glasses as a function of doped germanium and lithium oxide content. The Makishima-Makinzie model was applied to compute and estimate the investigated glass samples' mechanical properties. The optical features are studied by determining the optical energy gap ( $E_g$ ), Urbach energy ( $E_u$ ) of the TLGe glass system. Both factors vary with the content of dopant germanium and lithium ions in non-linear correlation. Refractive index, molar refraction, electronic polarizability, reflectivity, reflection factor are computed for the studied glasses. The metallization and dielectric constant for the prepared glasses are estimated. The obtained results depict the variation of the optical parameters versus the  $\text{GeO}_2 + \text{Li}_2\text{O}$  content change. The investigated glasses can be suitable for applying in optical devices. The examination showed that the replacement of  $\text{TeO}_2$  by  $\text{GeO}_2 + \text{Li}_2\text{O}$  enhances the investigated glass samples' shielding properties. The mass attenuation coefficient improved in order 41.79, 42.31, 42.91, and 42.96  $\text{cm}^2/\text{g}$  with substitution

Address correspondence to E-mail: mokhamed.khanfi@urfu.ru; m.nuc2012@gmail.com

## 1 Introduction

The interaction of ionizing radiation, which carries high energy with a medium, is very important in space technology, nuclear engineering, radiation medicine, radiotherapy, and other fields. Glassy materials have dual functions of being transparent to the light and absorbing the ionizing radiation, therefore providing protection from the photons for experimenters, observers, workers, and patients [1–4]. In the last few years, researchers have focused on developing different glass types that have appropriate shielding properties and can provide adequate protection from radiation [5–9]. It is essential to mention that fabricating new glasses for the shielding aims, possessing the desired shielding features, is still slow since it needs to overcome some difficulties. The reason for the slow production of new types of glass used in radiation protection is the necessity to have other properties for the prepared glasses. They must have suitable mechanical, thermal, chemical, and optical properties [10–12]. In particular, heavy metal oxides (HMO)-based glasses are favorable in radiation shielding applications because of their high density and highly effective atomic number. Different researchers also found that the glasses with HMO have a low mean free path and high radiation protection efficiency [13–16].

Glass formers, or glass network formers, are metal oxides within a glass composition that form the glass system network's interconnected backbone. The former glass germanate ( $\text{GeO}_2$ ) has a high density, good chemical durability, and great thermal stability, which helps stabilize the glass composition and improve the glass system's chemical and thermal properties. The oxide has been paired up with borate to create boro-germanate glasses, which have a high solubility with other metals, good thermal stability, transparency, resistance to moisture, and a low melting point. Meanwhile,  $\text{GeO}_2$ - $\text{SiO}_2$  glasses have shown to have a strong network and mechanical properties. Additionally, structurally,  $\text{GeO}_2$  has fewer vibrational frequencies than other metal oxide glasses. Recent studies have also explored the potential of  $\text{GeO}_2$ - $\text{TeO}_2$  glasses for applications in the industry [17, 18].

Tellurite ( $\text{TeO}_2$ ) can act as a glass modifier (an oxide that alters the glass network but is not part of the system's backbone) and glass former the composition of the glasses. Tellurite glasses have proven

to have advantageous features such as good chemical stability, and a high density, making it a heavy metal oxide. Since tellurite is an intermediate, however, the oxide on its own does not form a stable glass system because of its weak connectivity. Other metal oxides are typically paired with  $\text{TeO}_2$  to create a stable glass network because of this property. The germanate-tellurite combination, for instance, enhances the chemical resistance and thermal stability of the glass system. It creates glasses with unique optical and structural properties due to the existence of structural units such as  $\text{TeO}_3$ ,  $\text{TeO}_4$ ,  $\text{GeO}_3$ , and  $\text{GeO}_4$ . Because of these oxides' many desirable properties,  $\text{GeO}_2$ - $\text{TeO}_2$  glasses with additional oxides have recently gained much attention from researchers [19–21]. Different researchers recently found that the dense  $\text{TeO}_2$  and  $\text{GeO}_2$  glass systems are good candidates for radiation shielding purposes and are undoubtedly planned for radiation protection applications [3, 17, 18].

The present study aims to estimate the optical, mechanical, and radiation shielding properties of a glasses contains  $\text{TeO}_2$ ,  $\text{Li}_2\text{O}$ , and  $\text{GeO}_2$  compounds. The mechanical properties examined using the Makishema–Makinazie (M–M) model. Besides, the beneficial Monte-Carlo simulation code was utilized to estimate the radiation shielding properties of the investigated glass system.

## 2 Materials and methods

### 2.1 Mechanical properties

The hardness and elastic properties are fundamental to achieve suitable performance shielding materials. Thus, the mechanical properties and elastic moduli were theoretically estimated for the glass system contain  $\text{TeO}_2$ ,  $\text{Li}_2\text{O}$ , and  $\text{GeO}_2$  compounds with various ratios using the M–M model. The glass samples were coded in the present study as TLGe10, TLGe15, and TLGe20. The chemical composition (mol%) and density ( $\rho$ ,  $\text{g}/\text{cm}^3$ ) of the fabricated samples were enlisted in Table 1 [22].

Starting from the constating compounds dissociation energy  $G_i$ , the total dissociation energies ( $G_t$ ,  $\text{kJ}/\text{cm}^3$ ) were computed for the tested samples. The packing factor ( $V_i$ ,  $\text{cm}^3/\text{mol}$ ) was also calculated for the investigated TLGe glasses. The packing density ( $V_t$ ) is based on the molecular weight ( $M_w$ ,  $\text{g}/\text{mol}$ ),

**Table 1** Chemical composition, density, molar volume of TLGe glass samples

Samples	Chemical composition (mol%)			Density (g/cm <sup>3</sup> )	Molar volume $V_M$ (cm <sup>3</sup> /mol)
	TeO <sub>2</sub>	Li <sub>2</sub> O	GeO <sub>2</sub>		
TLGe10	80	10	10	5.18	27.25
TLGe15	70	15	15	5.01	26.33
TLGe20	60	20	20	4.97	24.68

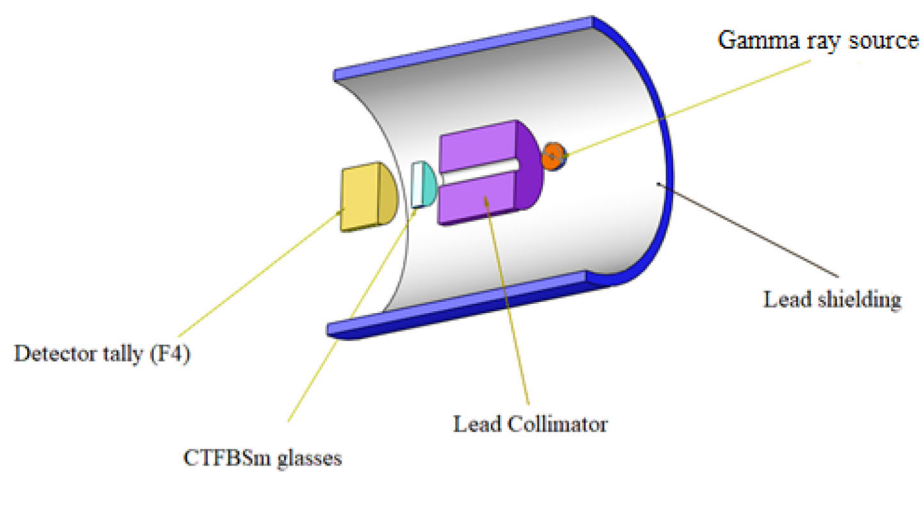
the molar fraction ( $x_i$ ), and the predicted values for  $V_i$  where  $V_t = (\rho/M_w)\sum v_i x_i$ . After that, the elastic moduli Young ( $Y$ , GPa), bulk ( $B$ , GPa), shear ( $S$ , GPa), and longitudinal ( $L$ , GPa) were computed using the estimated values of  $V_t$  and  $G_t$ , where  $Y = 2V_t G_t$ ,  $B = 1.2 V_t Y$ ,  $S = (3EB)/(9B - E)$ , and  $L = B + 0.75S$ . Moreover, the Poisson ratio ( $\sigma$ ) calculated from  $\sigma = 0.5 - 0.1388V_t$  and the micro harness ( $H$ , GPa) based on the computed  $\sigma$  values, where  $H = (1 - 2\sigma)/(6(1 + \sigma))$ . The softening temperature ( $T_s$ ), ultrasonic velocities ( $V_l$  and  $V_s$ ), and fractal bond connectivity ( $d$ ) were calculated [23–25].

## 2.2 Shielding capacity

The MCNP-5 code was applied to assess the protection parameters for the TLGe samples. The emitted gamma photons average track length (ATL) was simulated in the energy interval between 0.15 and 15 meV. An input file was created to achieve the required target. Figure 1 presented the 3D geometry that describes the created input file. The 3D geometry illustrates a big lead cylinder with a height of 500 mm and a diameter of 200 mm. This cylinder prevents the photons from escaping outside the geometry and

protects geometry from the surrounding background radiations. Inside this big cylinder, the radioactive source was placed in the center of this cylinder at point (0, 0, 0). The source type, dimensions, radioactivity distribution, and emission direction were introduced to the source specification card (SDEF). The photons emitted by the radioactive source were directed to the TLGe glass samples using a cylindrical collimator of lead with a height of 70 mm and a diameter of 10 mm. The collimator contains a vertical slit with a diameter of 10 mm to collimate the emitted photons. The glass samples were introduced to the input file as a small cylinder with a diameter of 15 mm and various thicknesses. The detector used in the present simulation has a type of F4 tally to estimate the number of photons incident per unit detector cell. The NPS card was set up to stop the interaction after  $10^6$  historical. The MCNP-5 code uses the photo atomic cross-section data from ENDF/B-VI.8 [26].

The simulated ATL was transferred to the linear attenuation coefficient (LAC,  $\mu$ ). From the LAC for the synthesized TLGe glasses, the mass attenuation coefficient (MAC,  $\mu_m$ ) was calculated where " $\mu_m = \mu\rho^{-1}$ ". Moreover, the transmission factor (TF, %) =

**Fig. 1** The 3D geometry representing the input file used in the present simulation

was calculated to describe the percentage of photons penetrated the glass thickness, where “TF = (1 - (I/I<sub>0</sub>)) × 100”. I<sub>0</sub> and I represent gamma-ray intensities’ values before and after passing the glass thickness [27, 28].

The BXCUM program is also a beneficial program utilized to compute the photons accumulated in the TLGe samples. The photons buildup describes the shielding parameters EBF and EABF, representing the exposure buildup factor and energy absorption buildup factor [29].

### 3 Results and discussion

#### 3.1 Mechanical properties

The glass density ρ (g/cm<sup>3</sup>) and molar volume (V<sub>M</sub>, cm<sup>3</sup>/mol) were determined and graphed in Fig. 2 as a function of the GeO<sub>2</sub> content. The V<sub>M</sub> is calculated based on the measured values of density where “V<sub>M</sub> = (M<sub>W</sub>/ρ)” and M<sub>W</sub> refers to the investigated glass samples’ theoretical molecular weight. Both ρ and V<sub>M</sub> were decreased by raising the TeO<sub>2</sub> substitution ratio. The illustrated reduction is due to replacement of TeO<sub>2</sub> with higher density (ρ = 5.67 g/cm<sup>3</sup> and M<sub>W</sub> = 159.6 g/mol) by GeO<sub>2</sub> (ρ = 4.25 g/cm<sup>3</sup> and M<sub>W</sub> = 104.61 g/mol) and Li<sub>2</sub>O (ρ = 2.01 g/cm<sup>3</sup> and M<sub>W</sub> = 29.88 g/mol). The glass ρ reduces from 5.18 to 4.97 g/cm<sup>3</sup>, and the V<sub>M</sub> decreased from 27.24 to 24.68 cm<sup>3</sup>/mol. The increment of GeO<sub>2</sub>- + Li<sub>2</sub>O in TLGe glasses leads to the molecular weight reduction due to the insertion of lighter Ge<sup>2+</sup>

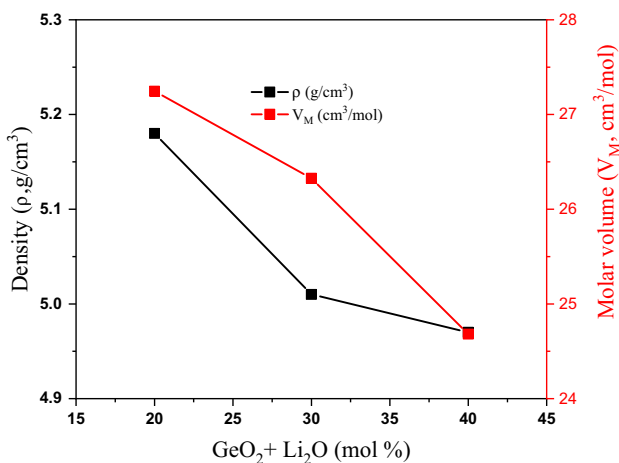


**Fig. 2** Variation of the molar volume and density of the fabricated glass samples with GeO<sub>2</sub> + Li<sub>2</sub>O content

ions and Li, and the density diminishes. Consequently, this procures to the increment of the molar volume.

The heat enthalpy (ΔH<sub>f</sub>) and the ionic radius (R) were used to calculate the studied glass samples’ G<sub>t</sub> and V<sub>i</sub>. The G<sub>t</sub> and V<sub>i</sub>’s calculated values were presented in Fig. 3 versus the (GeO<sub>2</sub> + Li<sub>2</sub>O) contents. The V<sub>i</sub> values decrease between 13.98, 13.62, and 13.26 cm<sup>3</sup>/mol while the G<sub>t</sub> exceeds in the order 55.48, 56.22, and 56.96 kJ/cm<sup>3</sup>. The observed behavior is related to V<sub>i</sub> and G<sub>i</sub> for the glass constituent TeO<sub>2</sub>, Li<sub>2</sub>O, and GeO<sub>2</sub>. In the present work, the TeO<sub>2</sub> (V<sub>i</sub> = 14.7 cm<sup>3</sup>/mol and G<sub>i</sub> = 54 kJ/cm<sup>3</sup>) replaced by the Li<sub>2</sub>O (V<sub>i</sub> = 8 cm<sup>3</sup>/mol and G<sub>i</sub> = 77.9 kJ/cm<sup>3</sup>) and GeO<sub>2</sub> (V<sub>i</sub> = 14.2 cm<sup>3</sup>/mol and G<sub>i</sub> = 44.9 kJ/cm<sup>3</sup>). As a result, the Te–O bond was replaced by stronger bonds Li–O and Ge–O bonds (Figs. 4, 5).

The V<sub>i</sub> values were utilized to calculate the V<sub>t</sub> of the studied samples. The calculated V<sub>t</sub> values for the TLGe glasses were calculated and tabulated in Table 2. The elastic moduli (Y, B, S, and L) were calculated and plotted versus the V<sub>t</sub> values. The elastic moduli increased between 56.93–61.20 GPa, 35.05–39.45 GPa, 23.15–24.64 GPa, and 65.93–72.32 GPa with increasing the V<sub>t</sub> of the glass samples between 0.513 and 13.26 for Y, B, S, and L, respectively. The estimated values for the TLGe glasses compared to elastic moduli were measured experimentally for some previously prepared glasses (see Table 3). The elastic moduli’s estimated values using the M–M model agree with those experimentally measured to 35V<sub>2</sub>O<sub>5</sub> + (55 - x)TeO<sub>2</sub> + xLi<sub>2</sub>O [30].

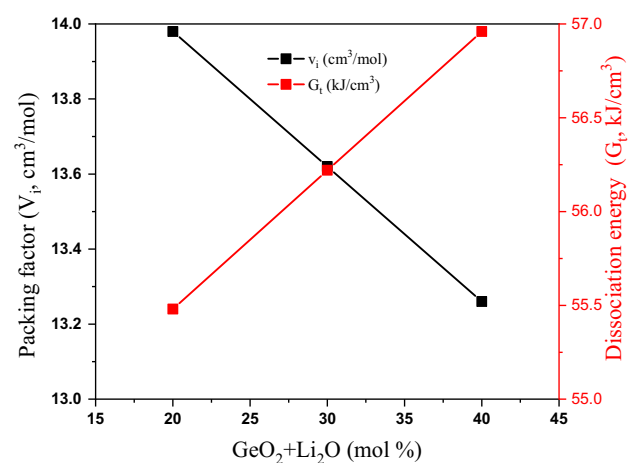


**Fig. 3** Variation of the glasses packing factor (V<sub>i</sub>) and dissociation energy (G<sub>t</sub>) versus the GeO<sub>2</sub> + Li<sub>2</sub>O content

Also, both  $\sigma$  and  $H$  are observed to increase with raising the  $\text{TeO}_2$  substitution ratio. The  $\sigma$  was increased in the order 0.229, 0.231, and 0.241, besides the  $H$  increased between 4.17, 4.22, and 4.24 GPa with raising the  $\text{GeO}_2 + \text{Li}_2\text{O}$  between 20, 30, and 40 mol%, respectively. As early discussed, the Te–O bonds' replacement with stronger Ge–O or Li–O bonds increases the  $G_t$  while reducing the  $V_i$  of the

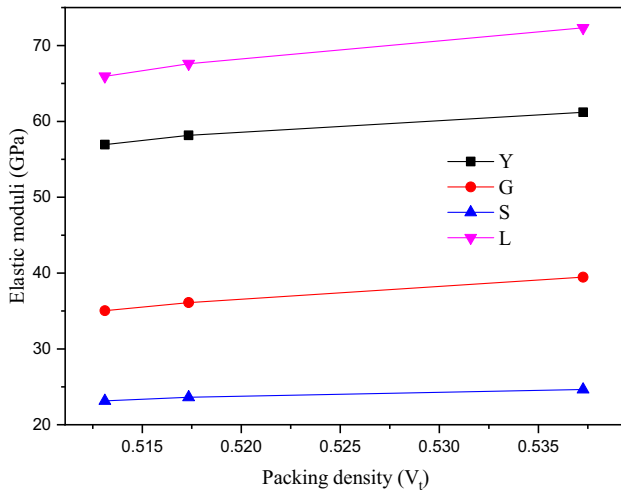


**Fig. 4** The elastic moduli versus the packing density ( $V_1$ ) and dissociation energy ( $G_t$ ) of the TLG samples

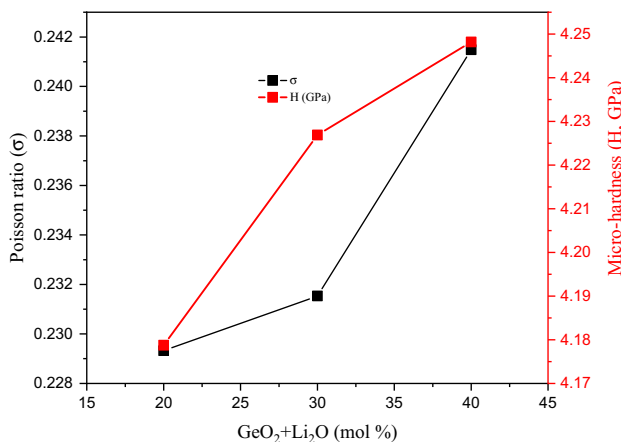


**Fig. 5** Variation of the micro-hardness and the Poisson ratio as a function of the  $\text{GeO}_2 + \text{Li}_2\text{O}$  content

**Table 2** Some physical properties for the studies TLGe glass samples

Sample code	$M_w$ (g/mol)	$V_t$	$V_1$ (m/s)	$V_s$ (m/s)	$T_s$ (K)	$d$
TLGe10	141.13	0.51	3567.69	2114.35	240.05	2.64
TLGe15	131.90	0.52	3673.34	2171.17	244.59	2.62
TLGe20	122.66	0.54	3814.77	2227.04	245.25	2.50

investigated TLGe glass samples. The elastic moduli increase with raising the  $\text{Te}_2\text{O}$  substitution. Hence, the  $\sigma$  and  $H$  depended on  $Y$  and  $S$  moduli. Thus,  $\sigma$  and  $H$  increase with raising the  $\text{GeO}_2 + \text{Li}_2\text{O}$  content in the investigated samples.

The calculated values of  $T_s$  and  $d$  were listed in Table 2, where the  $T_s$  were observed to increase in the order 240, 244, and 245 with increasing the  $\text{GeO}_2 + \text{Li}_2\text{O}$  content. The observed increase may be due to the high melting point (MP) of  $\text{GeO}_2$  and  $\text{Li}_2\text{O}$  ( $\text{MP}_{\text{GeO}_2} = 1115$  °C and  $\text{MP}_{\text{Li}_2\text{O}} = 1438$  °C) comparing to the  $\text{TeO}_2$  MP ( $\text{MP}_{\text{TeO}_2} = 732$  °C). The  $d$  values varied between 2.64, 2.62, and 2.5, and they were close to 3. Thus, the investigated glass samples have 3D networks of tetrahedral coordination polyhedral [31, 32].

In the present study,  $V_1$  and  $V_s'$  values were calculated based on  $L$  and  $S$  elastic moduli; they are enlisted in Table 2. The  $V_1$  varied in the range between 3567 and 3814 m/s, and  $V_s$  increased in the range between 2114 and 2227 m/s with raising the  $\text{GeO}_2 + \text{Li}_2\text{O}$  ratio between 20 and 40 mol%, respectively. The calculated values of  $V_1$  and  $V_s$  compared to some previously measured similar glasses as in Table 3. The estimated and measured values are in good agreement. This agreement between the theoretical and experimental measurements confirmed the M–M mode's ability to predict the mechanical properties of similar glasses containing  $\text{TeO}_2$ ,  $\text{Li}_2\text{O}$ , and  $\text{GeO}_2$ .

### 3.2 Optical features of the studied glasses

Based on the absorbance spectra for TLGe glasses, the absorption coefficient  $\alpha$  is estimated using Tauc expression [56] and modified by of Davis and Mott [33] for various optical transitions.

$$\alpha(h\nu) = [A(h\nu - E_g)]^{1/n}. \quad (1)$$

The value of  $n$  is an index with different values 1/2, 2 related to indirect and direct allowed transitions, and 3/2 and 3 for indirect and direct forbidden

**Table 3** Compare the elastic properties of the studied samples (using the M–M model) with some of previously fabricated glasses (using experimental ultrasonic velocities measurements)

Sample codes	Density (g/cm <sup>3</sup> )	Molar volume (cm <sup>3</sup> /mol)	V <sub>l</sub> (m/s)	V <sub>s</sub> (m/s)	Y (GPa)	B (GPa)	S (GPa)	L (GPa)	σ	H (GPa)	T <sub>s</sub> (K)
TLGe10	5.18	27.25	3567	2114	56.9	35.0	23.1	65.9	0.22	4.17	240
TLGe20	4.97	24.68	3814	2171	61.2	39.4	24.6	72.3	0.24	4.24	241
10 [28]	4.26	36.00	3510	2130	47	19.3	26.7	52.5	0.21	3.8	238
20 [28]	4.10	34.50	4090	2270	54	21.1	40.8	68.8	0.28	3.1	241

gap transitions. Figure 6a–c reveals the indirect transition of Tauc’s plot between  $[\alpha(h\nu)]^{1/2}$  with the incoming photon energy ( $h\nu$ ). The optical energy gap ( $E_g$ ) between valence and conduction bands can acquire from the prolongation of the linear fitting of Tauc’s plot to intercept the  $x$ -axis at  $[\alpha(h\nu)]^{1/2}$  equal zero. Figure 6d illustrates the  $E_g$  values vary non-linearly with the increment of  $\text{GeO}_2 + \text{Li}_2\text{O}$  content in TLGe glasses. It is clarified that, initially, the  $E_g$

value diminishes at  $x = 0.15$ . This decrement is owing to the disturbance in the network of glass and the modification in glass structures. The addition of  $\text{GeO}_2$  in lithium–tellurite glasses leads to the elongation fluctuation of tetrahedra non-bridging oxygen (NBOs) ( $\text{Ge-O}$  bond). Additionally, the deforming ( $\text{O-Ge-O}$  bond) vibrations with tetrahedral coordination. Yankov et al. [22] reported that FTIR of TLGe 10, 15, and 20 displays strong and weak band which

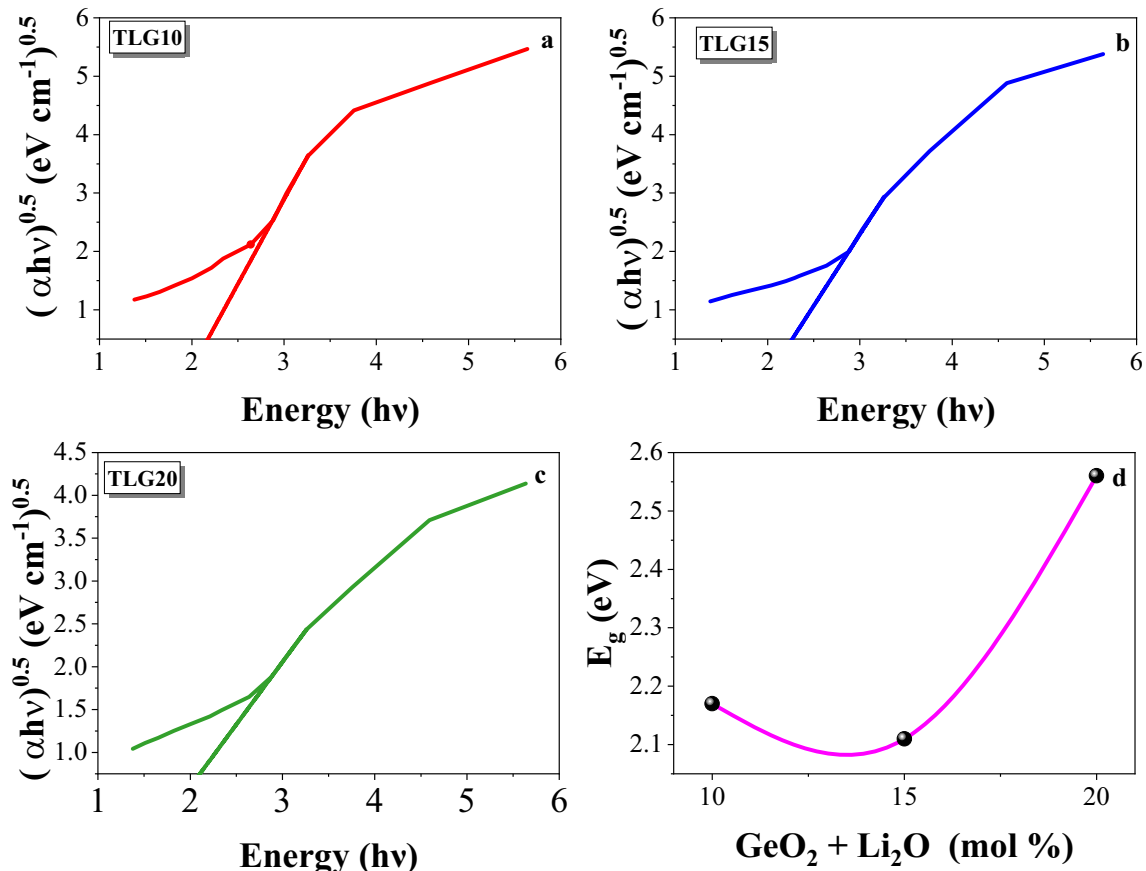


**Fig. 6** a–c represent the dependence of  $(\alpha h\nu)^{0.5}$  on the photon energy ( $h\nu$ ) for the TLG samples; inset shows the  $\text{GeO}_2 + \text{Li}_2\text{O}$  content, d dependence of the optical energy gap

attributed to Te–O bond stretching vibrations: trigonal bipyramids ( $\text{TeO}_4$ ) and trigonal pyramids ( $\text{TeO}_3$ ) units. Besides, the band is contributed from Te–O–X, Ge–O–X ( $X = \text{Te}$ , or  $\text{Ge}$ ) bending vibrations and associated from uniform stretching of  $\text{GeO}_4$ . After that, the  $E_g$  increases at TLGe20, where the alteration attributed to the structural diversity in TLGe glass structure with the variation in the molar volume of  $\text{GeO}_2$ .

To describe the disorder in the studied amorphous glass, the Urbach energy ( $E_u$ ) is detected where the higher values refer to the major disorder in the glass system and tend to appear defect [34, 35]. The Urbach energy can be computed based on Urbach Eq. (2) [35] is given by:

$$\ln(\alpha) = \ln(\alpha_0) + \frac{h\nu}{E_u}, \quad (2)$$

where  $\alpha$  refers to the absorption coefficient,  $\alpha_0$  is the stationary constant, and  $E_u$  is the Urbach energy. Figure 7a–c describe the variation of  $\ln(\alpha)$  against photon energy ( $h\nu$ ) with various  $\text{GeO}_2$  content in

TLGe glasses. The slope reciprocal of the correlation is intercepted at the Y-axis equal to zero. Thus, the values of  $E_u$  can be extracted. Figure 7d shows the  $E_u$  values vary in a non-linearly fashion with the increment of  $\text{GeO}_2 + \text{Li}_2\text{O}$  content due to the rise of the defects number in the TLGe glasses network [36, 37]. At TLGe15, the highest  $E_u$  value indicates that altering the weak bonds in the mentioned glass to the defects [38]. The obtained results are consistent with the XRD patterns of the studied glasses which cited from Ref. [22]. The results illustrate the amorphous nature of the examined glasses.

The refractive index is an important optical parameter that is affected by the glass chemical composition [39]. The refractive index for the studied glasses is computed using formula (3):

$$\frac{n^2 - 1}{n^2 + 2} = 1 - \left(\frac{E_g}{20}\right)^{1/2}. \quad (3)$$

Figure 8 reveals the refractive index values vary in decrement with the variation of  $\text{GeO}_2 + \text{Li}_2\text{O}$  content in the TLGe glasses. The density values of TLGe

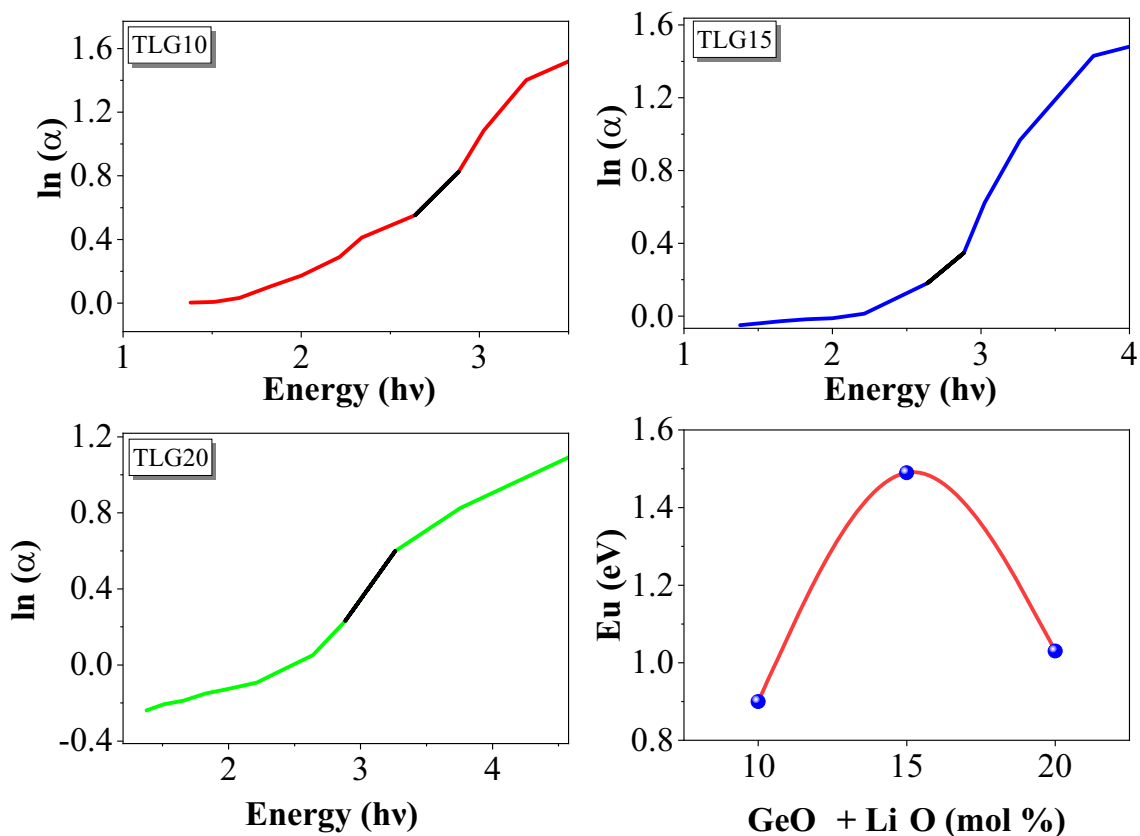


**Fig. 7** a–c Depict the variation of  $\ln(\alpha)$  of all compositions with photon energy. d Variation of Urbach energy with the concentration of  $\text{GeO}_2 + \text{Li}_2\text{O}$

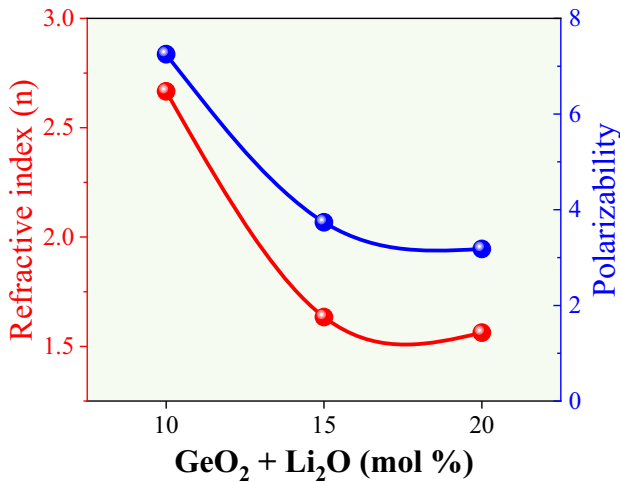


**Fig. 8** Variation of refractive index and polarizability with the concentration of GeO<sub>2</sub> + Li<sub>2</sub>O

glasses reduce with the rise of the GeO<sub>2</sub> + Li<sub>2</sub>O content; therefore, glass material compactness diminishes. Consequently, this decrement is owing to the decrease of non-bridging oxygen (NBOs), the low oxide ion polarizability. It is also evident in Fig. 8 the electronic polarizability of the investigated glasses directly proportional with the refractive index, which is evidence of the obtained results [40].

The molar refraction ( $R_m$ ), electronic polarizability ( $\alpha_m$ ), reflectivity ( $R$ ), and the reflection factor ( $P$ ) values are computed using the following formulas [41, 42] and tabulated in Table 4:

$$R_m = V_m \left( \frac{n^2 - 1}{n^2 + 2} \right), \tag{4}$$

$$\alpha_m = \frac{R_m}{2.52}, \tag{5}$$

$$R = \left( \frac{(n^2 - 1)}{(n^2 + 2)} \right)^2, \tag{6}$$

$$P = \left( \frac{2n}{(n^2 + 1)} \right). \tag{7}$$

The values of molar refraction ( $R_m$ ) fall from 18.29 to 7.98 for TLGe10 and TLGe20, respectively. The reflectivity ( $R$ ) and the reflection factor ( $P$ ) values of the investigated glasses are calculated and tabulated in Table 4. Apparently, in Table 4, the  $R$  values lessen with the augmentation of the GeO<sub>2</sub> content in TLGe glasses while the  $P$  values rise with the increment of GeO<sub>2</sub> + Li<sub>2</sub>O concentration.

The metallization ( $M$ ) factor is detected using Eq. (8) [43].

$$M = 1 - \frac{R_m}{V_m}. \tag{8}$$

The metallization ( $M$ ) of the mentioned glasses is computed to check the studied glasses' conductivity.  $M$ 's values are situated between 0, which refers to the conductive state, and 1, which indicates the insulator state [44].

$M$ 's obtained results illustrate the TLGe10 glass is an insulator where the  $M$  value is closed to zero. In contrast, the high concentration of GeO<sub>2</sub> + Li<sub>2</sub>O in TLGe15 and TLGe20 leads to the elevation of  $M$  values between 0.67 and 0.68, respectively. Therefore, TLGe15 and TLGe20 glasses tend to the metal case. Where in the metal case, the free electrons have fluctuated under the application of electromagnetic waves. Consequently, the reflection of the incident light wave may be observed.

The dielectric constant is calculated using the Eq. (9) [45]:

$$\epsilon = n^2. \tag{9}$$

The dielectric constant values for the studied glasses are registered and systemized in Table 4. The trend of dielectric constant values is adverse with the metallization constant values. Thus, the boost of

**Table 4** Estimated values of refractive index ( $n$ ), dielectric constant ( $\epsilon$ ), polarizability ( $\alpha_e$ ), molar refraction ( $R_m$ ), metallization constant ( $M$ ), reflection factor ( $P$ ), Reflectivity ( $R$ ), for all prepared glass samples

x	Refractive index ( $n$ )	Dielectric constant ( $\epsilon$ )	Polarizability ( $\alpha_e$ )	Molar refraction ( $R_m$ )	Metallization constant ( $M$ )	Reflection factor ( $P$ )	Reflectivity ( $R$ )
TLGe10	2.67	7.13	7.26	18.29	0.33	0.66	0.21
TLGe15	1.58	2.50	3.49	8.79	0.67	0.90	0.06
TLGe20	1.56	2.43	3.17	7.98	0.68	0.91	0.05



GeO<sub>2</sub> + Li<sub>2</sub>O concentration in the studied glass causes a reduction of the dielectric constant. The dielectric features depend on the chemical composition and the material preparation. What's more, the dielectric constant impacted the material bonding (Table 5).

The third order non-linear optical susceptibility ( $\chi^{(3)}$ ) calculated based on the refractive index ( $n$ ) values and given by Eq. (10) [46, 47]:

$$\chi^{(3)} = \left[ \frac{(n^2 - 1)^4}{4\pi} \right] \quad (10)$$

The variation of  $\chi^{(3)}$  with the GeO<sub>2</sub> + Li<sub>2</sub>O content in the TLGe glasses is studied and presented in Fig. 9. The elevation of polarization and the formulation (TeO<sub>3</sub>)<sup>-2</sup> clusters in TLGe glasses' network increase the optical susceptibility. Meanwhile, the addition of GeO<sub>2</sub> + Li<sub>2</sub>O with high concentration procured to form defects in the glass matrix structure, which is accepted with the computed Urbach energy values.

The basicity is the optical parameter utilized to determine the acid–base features of glasses [48]. This depends on detecting the ion polarizability and the energy gap. Dimitrov and Komatsu [49] are predicted the electronic polarizability ( $\alpha_0^{2-}$ ) of oxygen ion using the following Eq. (11):

$$\alpha_0^{2-} = \left[ \frac{V_m}{2.52} \left( 1 - \sqrt{\frac{E_g}{20}} \right) - \sum p\alpha_i \right] q^{-1}, \quad (11)$$

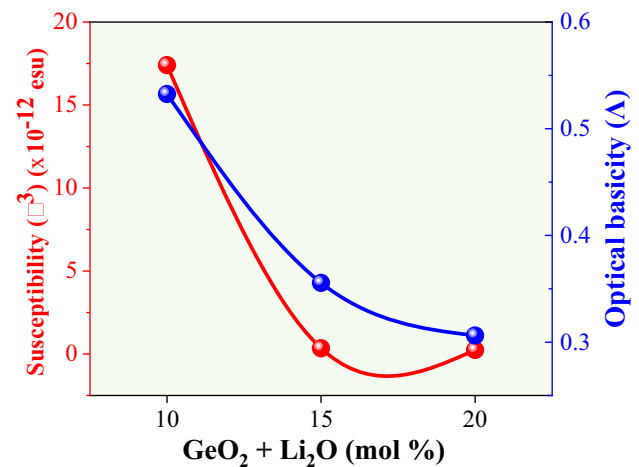


**Fig. 9** Variation of third-order non-linear susceptibility and optical basicity of the samples with the concentration of GeO<sub>2</sub> + Li<sub>2</sub>O

where  $E_g$  is the optical energy band gap,  $p$  and  $q$  are the cations number and oxide ions, respectively, in each chemical oxide  $A_pO_q$ .

Subsequently, the optical basicity ( $\Lambda$ ) values have been computed using the formula (12) [48, 50]:

$$\Lambda = 1.67 \left( 1 - \frac{1}{\alpha_0^{2-}} \right). \quad (12)$$

The dependence of optical basicity on the GeO<sub>2</sub> + Li<sub>2</sub>O content in TLGe glasses is explained in Fig. 9. It is recognized in Fig. 9 the values of optical basicity

**Table 5** The mass attenuation coefficient and the difference between MCNP and XCOM program

Energy (MeV)	Mass attenuation coefficient (cm <sup>2</sup> /g)								
	TLGe10			TLGe15			TLGe20		
	MCNP	XCOM	Diff (%)	MCNP	XCOM	Diff (%)	MCNP	XCOM	Diff (%)
0.015	41.7984	41.8300	- 0.0755	42.3179	42.3600	- 0.0995	42.9160	42.9600	- 0.1026
0.03	6.3983	6.4940	- 1.4953	6.4770	6.5670	- 1.3900	6.5679	6.6500	- 1.2502
0.15	0.5611	0.5130	8.5716	0.5372	0.4927	8.2905	0.5098	0.4694	7.9244
0.3	0.1553	0.1512	2.6619	0.1526	0.1485	2.6719	0.1451	0.1454	- 0.2299
0.6	0.0797	0.0799	- 0.3088	0.0795	0.0797	- 0.2908	0.0792	0.0794	- 0.2819
0.8	0.0663	0.0665	- 0.2321	0.0663	0.0665	- 0.2239	0.0663	0.0664	- 0.2178
1.5	0.0462	0.0467	- 1.1531	0.0463	0.0468	- 1.1091	0.0464	0.0469	- 1.0481
3	0.0358	0.0359	- 0.5202	0.0357	0.0359	- 0.5085	0.0356	0.0358	- 0.4922
5	0.0330	0.0331	- 0.2715	0.0328	0.0328	- 0.2735	0.0325	0.0326	- 0.2640
8	0.0332	0.0333	- 0.1899	0.0328	0.0329	- 0.1740	0.0323	0.0324	- 0.2018
10	0.0341	0.0342	- 0.1640	0.0336	0.0337	- 0.1588	0.0330	0.0331	- 0.1489
15	0.0368	0.0369	- 0.1122	0.0362	0.0362	- 0.1281	0.0354	0.0354	- 0.1316

drop from 0.53 to 0.3 with the germanium oxide content. The value of  $A$  indicates the ionic or covalent natures in the studied glasses [49]. Thus, the high value of  $A$  refers to the ionic bonding, whereas the small value mentions covalent bonding. In the present study, the optical basicity declines with the increment of germanium oxide, which indicates the rise of the covalent bonding in the TLGe glasses.

### 3.3 Shielding properties evaluation

The materials with diverse chemical compositions in recent years were developed for utilization in various radiation protection applications. Thus, shielding properties are important to investigate. Among these shielding parameters are the LAC, or  $\mu$  which was detected to measure glass material’s ability to attenuate the incoming gamma-ray. Figure 10 reveals the  $\mu$  of TLGe glasses’ variation with the incoming energies in the low range (0.015–1.5 meV). It is clarified in Fig. 10 the  $\mu$  values drop with the elevate of the incoming energy. The maximum values of the simulated  $\mu$  are evidenced in the photoelectric effect (PE) region, especially at low energy of 0.015 meV. An unforeseen increase in the  $\mu$  values in the PE region is observed. This is linked to the X-ray  $k$ -absorption edge of at 0.0318 meV for the tellurium (Te) [52]. Above 0.1 meV, the  $\mu$  values gradually reduce with the excess photon energy. This lessening is concerning the cross-section of the Compton scattering (CS),

which is inversely proportional with the photon energy ( $\sigma_{CS} \propto E^{-1}$ ) [52, 53].

The insertion of  $GeO_2 + Li_2O$  content in the binary lithium-tellurite glasses impacted the  $\mu$  values. Decreasing the  $TeO_2$  at the expense of  $GeO_2 + Li_2O$  leads to a decrease in molecular weight, and thus the  $Z_{eff}$  and the density of TLGe glasses will reduce. Figure 10 displays the  $\mu$  amount to the superior values diminished from 216.5 to 213.2  $cm^{-1}$  for TLGe10 and TLGe20, respectively, at low energy 0.015 meV. The  $\mu$  reaches the least values lessened from 0.239 to 0.230  $cm^{-1}$  TLGe10 and TLGe20, respectively, at high energy 1.5 meV. At low photon energy range, the  $\mu$  values increase by adding the germanium (Ge) content in the lithium tellurite glasses because the  $\mu$  of (Ge) is higher than the tellurite (Te), especially in between 0.015 and 0.04 meV. However, the atomic number of (Te) is high compared with the (Ge). On the other hand, it is found the  $\mu$  values tend to increase in the intermediate photon energies wherein the CS region is the triumphant and the  $\mu$  of Te is high compared with the Ge [7]. Thus, it is concluded the addition of  $GeO_2$  in the binary lithium-tellurite glasses will enhance the shielding factors like the  $\mu$  in the mentioned low energies, but it is not good applied at higher photon energies.

The investigated glass samples LAC were compared to some previously published germanate-based glass (TG1 and TG4) [54] besides the commercial shielding glasses (RS 253, RS 323 G19, RS 360, and RS 520) [55], as shown in Fig. 11. The investigated glass samples have

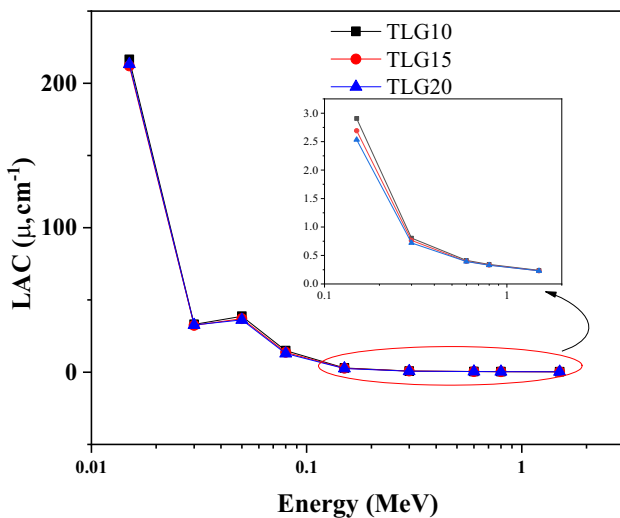


**Fig. 10** The linear attenuation coefficient ( $\mu$ ) as a function of the incoming photon energy and the  $GeO_2 + Li_2O$  concentrations in the prepared glasses

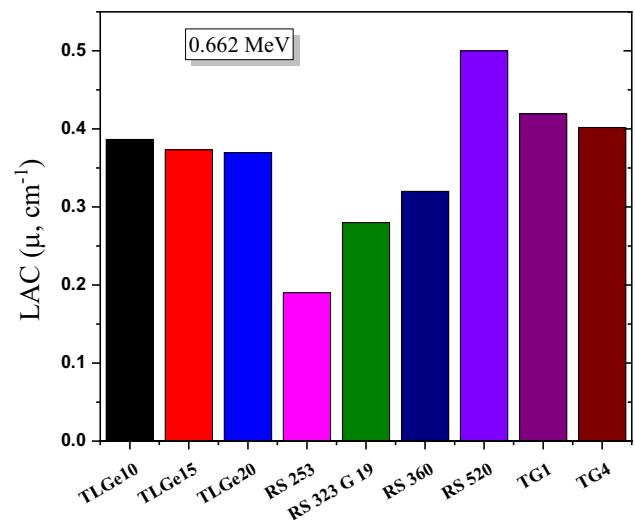


**Fig. 11** Comparison between investigated glass samples’ LAC and those of commercial and previously reported glass samples

LAC varied between 0.38658 and 0.369  $\text{cm}^{-1}$  for glass samples TLGe 5 and TLGe 15, respectively, at gamma photon energy 0.662 meV. These mentioned values are higher than the commercial shielding glasses RS 253, RS 323 G19, and RS 360, with values 0.19, 0.28, and 0.32  $\text{cm}^{-1}$ . On the other hand, the investigated glass samples' LAC is lower than the previously published glass TG1 and TG4 due to the high content of  $\text{TeO}_2$  and  $\text{GeO}_2$  in these glasses. Also, it is lower than the commercial glass sample RS 520, which has around 71% of PbO in its content.

The radiation shielding can impact the thickness of the investigated glass material. The applied thickness measures the ability of glass materials to prevent the incident photons transfer through the material. Thus, photons' transmission through the glass material thickness defines the transmission rate (TR) where it is computed and presented in Fig. 12. Figure 12 exhibits the dependence TR on the incoming photons energy and the thickness of glass material. The TR is studied at the selected gamma energy (0.15 and 1.5 meV) at various thicknesses 1, 2.5, and 5 cm to illustrate this effect. The values of TR are raised with the growth of incoming photons energy. At 0.15 meV, the maximum values of TR are appeared at TLGe20 varied from 0 to 7.94%, while the little values are

ranged from 0 to 5.47% for the TLGe10 glass. Moreover, at 1.5 meV, the TR values are varied between 30.3–78.7% and 31.6–79.4% for TLGe10 and TLGe20, respectively. The elevation of TR is due to the increase of incoming photons' ability to penetrate the glass material, and the gamma photon wavelength reduces ( $E = hc/\lambda$ ). Then the number of photons interactions within the TLGe material will diminish, and TR will increase.

The photon TR varied with the rise in the thickness of the studied glasses. Figure 12 displays at 1.5 meV, the TR values tend to drop from 79.4 to 31.6% with the increased thickness of TLGe20 glasses from 1 to 5 cm. This results in an increase in photon lifetime within the glass and increased photon buildup from scattering. In effect, the number of photon interactions increases, and the TR decreases.

The BXCUM program is employed to compute the additional radiation shielding parameters such as the equivalent atomic number ( $Z_{\text{eq}}$ ), EBF, EABF. The equivalent atomic number ( $Z_{\text{eq}}$ ) is calculated based on the studied glasses' mass attenuation coefficient and plotted against the incoming photon energies in Fig. 13. It is exhibited in Fig. 13 the minimum  $Z_{\text{eq}}$  values are founded in the PE region (0.015–0.1 meV), where they boost gradually with the elevation of the

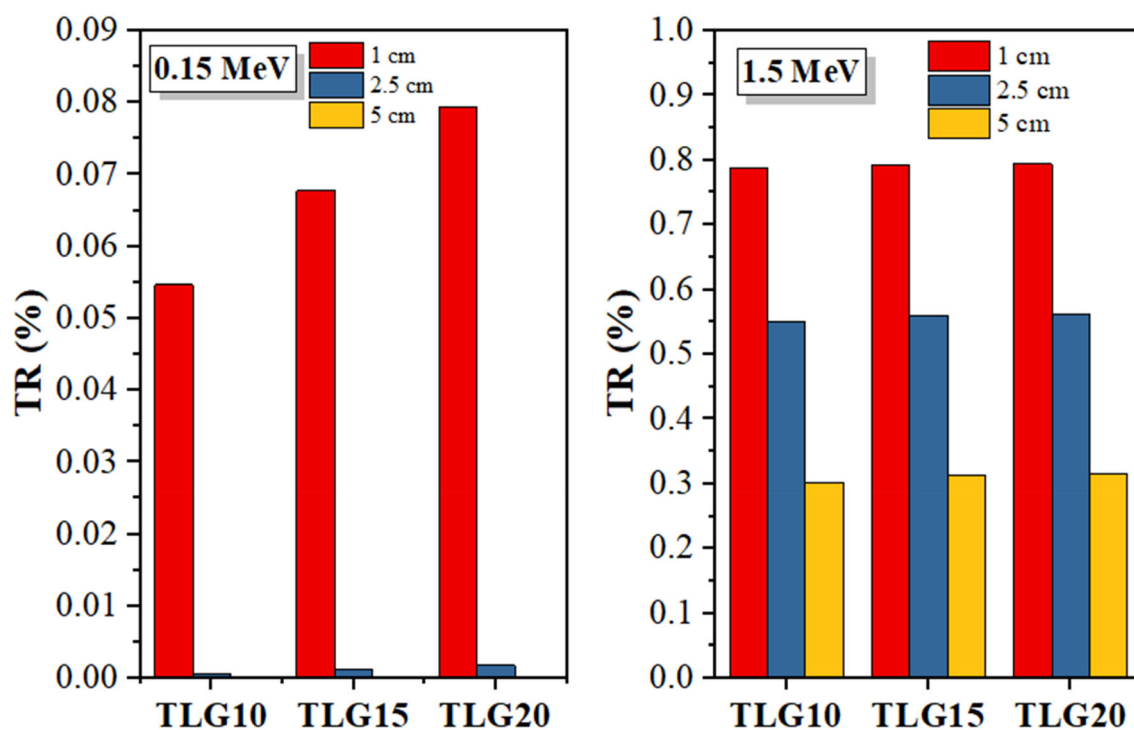
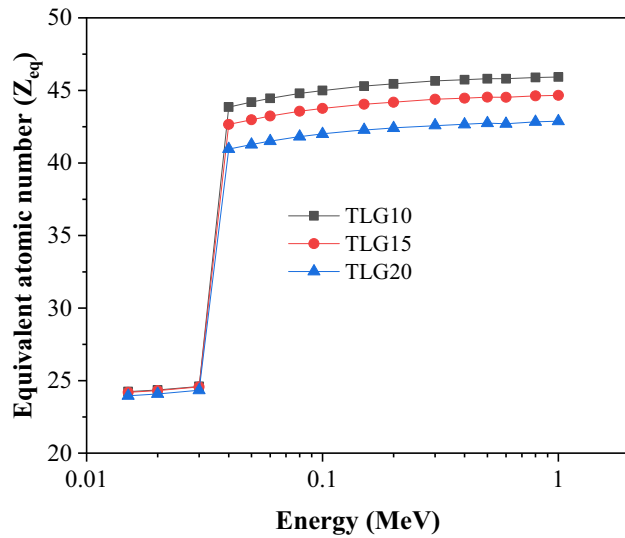


Fig. 12 The incoming gamma photons' transmission rate as a function of the glass thickness



**Fig. 13** The equivalent atomic number of the TLG glasses as a function of the incoming photon energy and the GeO<sub>2</sub> + Li<sub>2</sub>O concentration

incoming photon energies. Subsequently, in the CS region (above 0.1 meV), the incoming photon energy rises, but the Z<sub>eq</sub> tardily increases.

The EBF describes the passing of incoming photons through the glass material thickness and accumulation in the air. The accumulation number of photons inside the material thickness is detected with EABF. Therefore, the buildup factors EBF and EABF depend on the incoming photon energy and the penetration depth (PD). Figures 14, 15, 16 illustrate the EBF and EABF of the germanium according to lithium-tellurite glasses which have minimum values at the low incoming photon energies because of the PE interaction. The incoming photons are totally consumed of energy to expel the boundary electron. Thus, all photons are absorbed and are not accumulated inside the glass material. Around the photon energy, 0.04 meV sudden elevation of the EBF values is monitored for all germanium lithium-tellurite glasses. This is expected to the X-ray K-absorption edge for the tellurium (Te) [52]. Thus, K absorption edges' maximum values reduce with diminishing the tellurium oxide (TeO<sub>2</sub>) and increase the germanium and lithium oxides (GeO<sub>2</sub> + Li<sub>2</sub>O) in binary lithium-tellurite glasses. Then in the intermediate energy range,

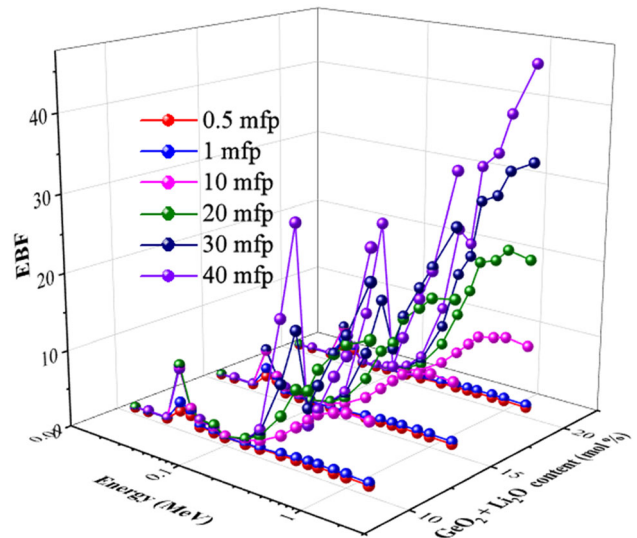


**Fig. 14** The exposure buildup factor as a function of the incoming gamma photon energies (0.015–1.5 meV) at some fixed penetration depths

the CS interaction is the epidemic. Therefore, the incident photons interactions will increase where photons will pass through the glass material, and the rest part will be stacked with the scattering photons. Consequently, EBF and EABF values increase.

The dependence of accumulation photons within the TLGe glasses is studied and presented in Figs. 15, 16, 17. It can be recognized of EBF and EABF variation rise slowly with the increase in penetration depth up to 10 mfp. The EBF and EABF reach the maximum at the PD = 20 mfp for all fabricated TLGe glasses. This is associated with the number of photons that expend long periods to penetrate the glass material thickness, and consequently, photons' interaction with the glass material increases. The lowest EBF and EABF are detected at PD = 0.5 mfp.

Additionally, it can be seen in the figures that the addition of GeO<sub>2</sub> + Li<sub>2</sub>O in the investigated glasses influenced EBF and EABF. The highest EBF and EABF are adjusted at the TLGe20 for all penetration depths in between (0.5–40 mfp). Meanwhile, the little values are predicted in TLGe10 glasses. Finally, it can be concluded that the replacement of TeO<sub>2</sub> with GeO<sub>2</sub> + Li<sub>2</sub>O will enhance the radiation shielding applications of TLGe glasses.

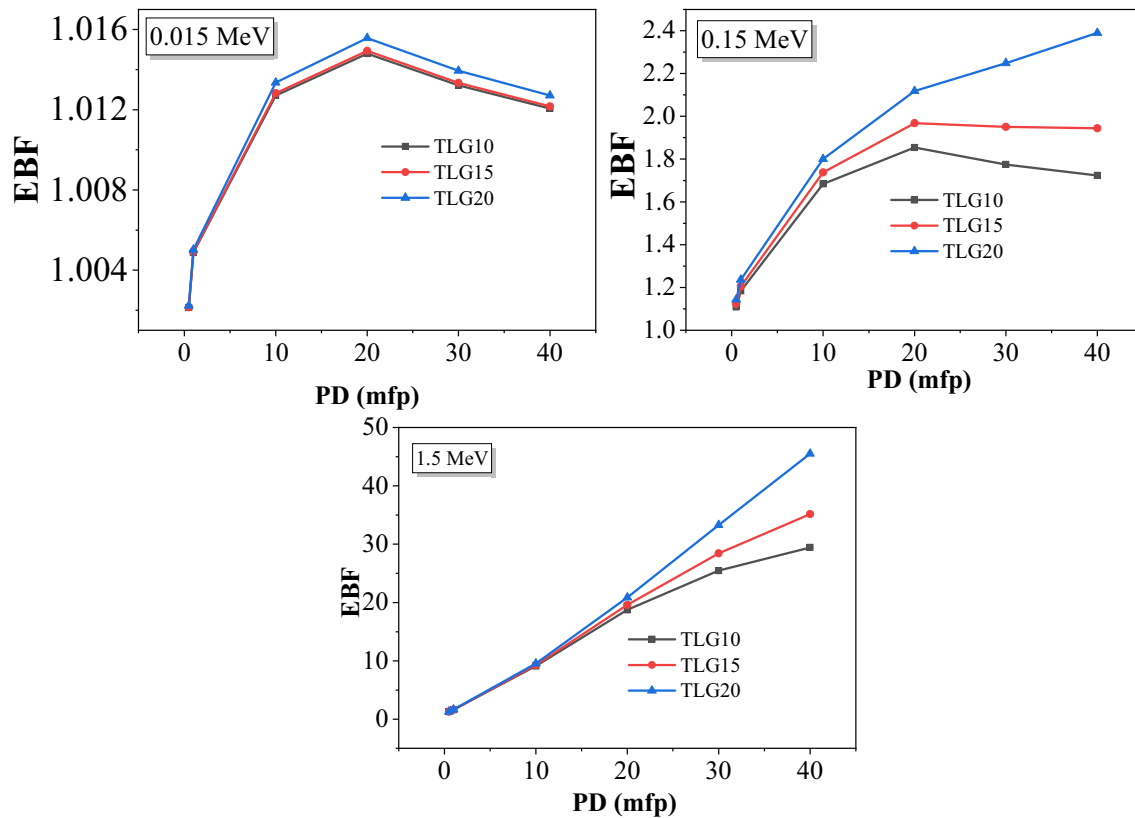


**Fig. 15** The EBF variation with the penetration depth of TLG glasses at various gamma photons energy

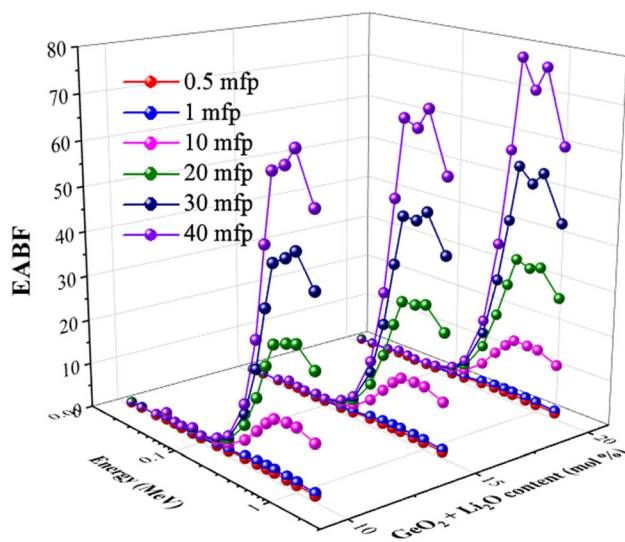


**Fig. 16** The variation of the energy absorption buildup factor as a function of the incoming gamma photon energies (0.015–1.5 meV) at some fixed penetration depths

## 4 Conclusions

The bandgap energy and Urbach energy reduces with the increment of the  $\text{GeO}_2 + \text{Li}_2\text{O}$  in the prepared glasses. The studied glasses are considered suitable candidates for applications in optics devices. Regarding the mechanical properties, the elastic moduli were enhanced and varied between 56.93–61.20 GPa (for Young), 35.05–39.45 GPa (for bulk), 23–25–24.64 GPa (for shear), and 65.93–72.32 GPa (for longitudinal). Moreover, the glasses micro-hardness increased between 4.17 and 4.24 GPa with raising the  $\text{GeO}_2 + \text{Li}_2\text{O}$  ratio between 20 and 40 mol%, respectively. Furthermore, studying the investigated glass samples' shielding capacity showed that the MAC progressed in the order 41.79, 42.31, 42.91  $\text{cm}^2/\text{g}$  with raising the  $\text{GeO}_2 + \text{Li}_2\text{O}$  insertion ratio between 20, 30, and 40 mol%, respectively. The results presented in this paper concluded

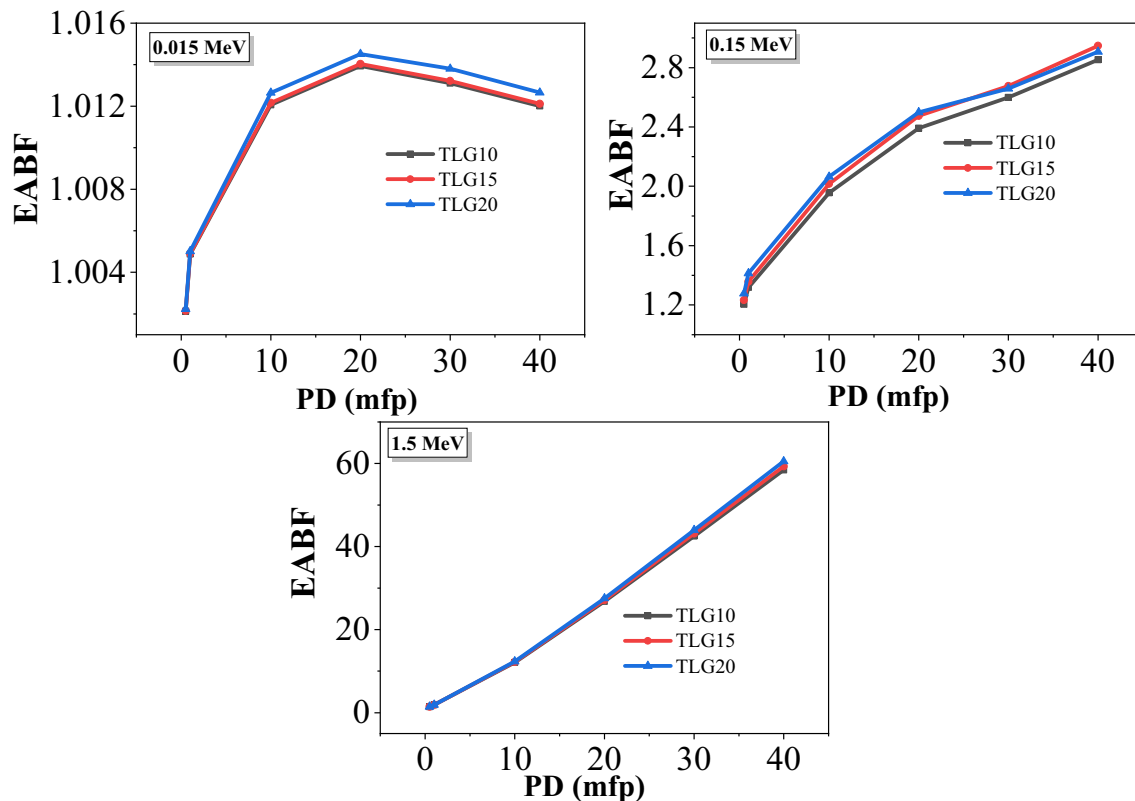


**Fig. 17** The EABF variation with the penetration depth of fabricated glasses at various gamma photons energy

that the substitution of TeO<sub>2</sub> by GeO<sub>2</sub> + Li<sub>2</sub>O enhances the investigated glass's optical, shielding, and mechanical properties. Thus, it is suitable for optical devices and radiation shielding applications, especially for low and mid energy regions.

## Acknowledgements

This research was funded by the Deanship of Scientific Research at Princess Nourah bint Abdulrahman University through the Fast-Track Research Funding Program.

## References

1. S. Ruengsri, Radiation shielding properties comparison of Pb-based silicate, borate, and phosphate glass matrices. *Technol. Nucl. Install. Sci.* (2014). <https://doi.org/10.1155/2014/218041>
2. S.R. Manohara, S.M. Hanagodimath, L. Gerward, Photon interaction and energy absorption in glass: a transparent gamma ray shield. *J. Nucl. Mater.* **393–3**, 65–472 (2009)
3. M.I. Sayyed, Y. Al-Hadeethi, M.M. AlShammari, M. Ahmed, S.H. Al-Heniti, Y.S. Rammah, Physical, optical and gamma radiation shielding competence of newly borotellurite based glasses: TeO<sub>2</sub>–B<sub>2</sub>O<sub>3</sub>–ZnO–Li<sub>2</sub>O<sub>3</sub>–Bi<sub>2</sub>O<sub>3</sub>. *Ceram. Int.* **47**, 611–618 (2021)
4. M.Y. Hanfi, I.V. Yarmoshenko, A.A. Seleznev, G. Malinovsky, E. Ilgasheva, M.V. Zhukovsky, Beta radioactivity of urban surface-deposited sediment in three Russian cities. *Environ. Sci. Pollut. Res.* **27**(32), 40309–40315 (2020). <https://doi.org/10.1007/s11356-020-10084-9>
5. H. Akyildirim, E. Kavaz, F.I. El-Agawany, E. Yousef, Y.S. Rammah, Radiation shielding features of zirconolite silicate glasses using XCOM and FLUKA simulation code. *J. Non-Cryst. Solids* **545**, 120245 (2020)
6. S. Yasmin, B.S. Barua, M.U. Khandaker, M.A. Rashid, D.A. Bradley, M.A. Olatunji, M. Kamal, Studies of ionizing radiation shielding effectiveness of silica-based commercial glasses used in Bangladeshi dwellings. *Results Phys.* **9**, 541–549 (2018)
7. M.I. Sayyed, R. El-Mallawany, Shielding properties of (100–x) TeO<sub>2</sub>–(x)MoO<sub>3</sub> glasses. *Mater. Chem. Phys.* **201**, 50–56 (2017)
8. M.I. Sayyed, A.H. Almuqrin, R. Kurtulus, A.M.V. Javier-Hila, K. Kaky, T. Kavas, X-ray shielding characteristics of

- P2O<sub>5</sub>–Nb2O<sub>5</sub> glass doped with Bi2O<sub>3</sub> by using EPICS2017 and Phy-X/PSD. *Appl. Phys. A* **127**, 243 (2021)
9. S.A.M. Issa, M.I. Sayyed, M.H.M. Zaid, K.A. Matori, Photon parameters for gamma-rays sensing properties of some oxide of lanthanides. *Results Phys.* **9**, 206–210 (2018)
  10. A.S. Abouhaswa, E. Kavaz, A novel B<sub>2</sub>O<sub>3</sub>–Na<sub>2</sub>O–BaO–HgO glass system: synthesis, physical, optical and nuclear shielding features. *Ceram. Int.* **46**, 16166–16177 (2020)
  11. E. Kavaz, E.H. Ghanim, A.S. Abouhaswa, Optical, structural and nuclear radiation security properties of newly fabricated V<sub>2</sub>O<sub>5</sub>–SrO–PbO glass system. *J. Non-Cryst. Solids* **538**, 120045 (2020)
  12. M.I. Sayyed, K.A. Mahmoud, E. Lacomme, M.M. AlShammari, N. Dwaikat, Y.S.M. Alajerami, M. Alqahtani, B.O. Elbashir, M.H.A. Mhareb, Development of a novel MoO<sub>3</sub>-doped borate glass network for gamma-ray shielding applications. *Eur. Phys. J. Plus* **136**, 108 (2021)
  13. M. Kurudirek, Heavy metal borate glasses: potential use for radiation shielding. *J. Alloys Compd.* **727**, 1227–1236 (2017)
  14. K. Kirdsiri, J. Kaewkhao, A. Pokaipisit, W. Chewpraditkul, P. Limsuwan, Gamma-rays shielding properties of xPbO:(100 x)B<sub>2</sub>O<sub>3</sub> glasses system at 662 keV. *Ann. Nucl. Energy* **36**, 1360–1365 (2009)
  15. A.H. Almuqrin, M.I. Sayyed, Radiation shielding characterizations and investigation of TeO<sub>2</sub>–WO<sub>3</sub>–Bi<sub>2</sub>O<sub>3</sub> and TeO<sub>2</sub>–WO<sub>3</sub>–PbO glasses. *Appl. Phys. A* **127**, 190 (2021)
  16. R. Kurtulus, T. Kavas, I. Akkurt, K. Gunoglu, An experimental study and WinXCom calculations on X-ray photon characteristics of Bi<sub>2</sub>O<sub>3</sub>- and Sb<sub>2</sub>O<sub>3</sub>-added waste soda-lime-silica glass. *Ceram. Int.* **46**, 21120–21127 (2020)
  17. K.M. Kaky, M.I. Sayyed, A.A. Ati, M.H.A. Mhareb, K.A. Mahmoud, S.O. Baki, M.A. Mahdi, Germanate oxide impacts on the optical and gamma radiation shielding properties of TeO<sub>2</sub>–ZnO–Li<sub>2</sub>O glass system. *J. Non-Cryst. Solids* **546**, 120272 (2020)
  18. M.I. Sayyed, K.M. Kaky, E. Şakar, U. Akbaba, M.M. Taki, O. Agar, Gamma radiation shielding investigations for selected germanate glasses. *J. Non-Cryst. Solids* **512**, 33–40 (2019)
  19. M. Kumar, Y.C. Ratnakaram, Role of TeO<sub>2</sub> coordination with the BaF<sub>2</sub> and Bi<sub>2</sub>O<sub>3</sub> on structural and emission properties in Nd<sup>3+</sup> doped fluorophosphate glasses for NIR 1.058 µm laser emission. *Opt. Mater.* **112**, 110738 (2021)
  20. C.B. Deng, M. Zhang, T. Lan, M.J. Zhou, Y. Wen, J. Zhong, X.Y. Sun, Spectroscopic investigation on Eu<sup>3+</sup>-doped TeO<sub>2</sub>–Lu<sub>2</sub>O<sub>3</sub>–WO<sub>3</sub> optical glasses. *J. Non-Cryst. Solids* **554**, 120565 (2021)
  21. V.A.G. Rivera, D. Manzani, V.A.G. Rivera, *Technological Advances in Tellurite Glasses*, Springer International Publishing (2017)
  22. G. Yankov, L. Dimowa, N. Petrova, M. Tarassov, K. Dimitrov, T. Petrov, B.L. Shivachev, Synthesis, structural and non-linear optical properties of TeO<sub>2</sub>–GeO<sub>2</sub>–Li<sub>2</sub>O glasses. *Opt. Mater.* **35**, 248–251 (2012)
  23. E.S. Yousef, A. El-Adawy, N. El-KheshKhany, Effect of rare earth (Pr<sub>2</sub>O<sub>3</sub>, Nd<sub>2</sub>O<sub>3</sub>, Sm<sub>2</sub>O<sub>3</sub>, Eu<sub>2</sub>O<sub>3</sub>, Gd<sub>2</sub>O<sub>3</sub> and Er<sub>2</sub>O<sub>3</sub>) on the acoustic properties of glass belonging to bismuth-borate system. *Solid State Commun.* **139**, 108–113 (2006)
  24. A. Makishima, J.D. Mackenzie, Direct calculation of Young's modulus of glass. *J. Non-Cryst. Solids.* **12**, 35–45 (1973)
  25. A. Makishima, J.D. Mackenzie, Calculation of bulks modulus, shear modulus and Poisson's ratio of glass. *J. Non-Cryst. Solids.* **17**, 147–157 (1975)
  26. X-5 Monte Carlo Team, MCNP-A General Monte Carlo N-Particle Transport Code, Version 5, Los Alamos Controlled Publication. LA-CP-03-0245 (2003)
  27. K.A. Mahmoud, M.I. Sayyed, A.M. Alhuthali, M.Y. Hanfi, The effect of CuO additive on the mechanical and radiation shielding features of Li<sub>2</sub>B<sub>4</sub>O<sub>7</sub>–Pb<sub>2</sub>O<sub>3</sub> glass system. *Boletín de la Sociedad Española de Cerámica y Vidrio* (2021). <https://doi.org/10.1016/j.bsecv.2020.11.005>
  28. K.M. Kaky, M.I. Sayyed, M.H.A. Mhareb, A. Abdalsalam, K.A. Mahmoud, S.O. Baki, M.A. Mahdi, Physical, structural, optical and gamma radiation attenuation properties of germanate-tellurite glasses for shielding applications. *J. Non-Cryst. Solids* **545**, 120250 (2020)
  29. Ö. Eyecioğlu, A.M. El-Khayatt, Y. Karabul, M. Çağlar, O. Toker, O. İçelli, BXCCom: a software for computation of radiation sensing. *Radiat. Eff. Defects Solids.* **174**, 506–518 (2019)
  30. S. Laila, A.K. Suraya, A.K. Yahya, Effect of glass network modification on elastic and structural properties of mixed electronic-ionic 35V<sub>2</sub>O<sub>5</sub>–(65-x)TeO<sub>2</sub>–(x)Li<sub>2</sub>O glass system. *Chalcogenide Lett.* **11-2**, 91–104 (2014)
  31. D.J. Bergman, Y. Kantor, *Phys. Rev. Nature* **207**, 1238 (1965)
  32. G.A. Saunders, T. Brennan, M. Acet, M. Cankurtaran, H.B. Senin, H.A.A. Sidek, M. Federico, Elastic and non-linear acoustic properties and thermal expansion of cerium metaphosphate glasses. *J. Non-Cryst. Solids.* **282**, 291–305 (2001)
  33. N.F. Mott, E.A. Davis, conduction in non-crystalline systems V conductivity, optical absorption and photoconductivity in amorphous semiconductors. *Philos. Mag.* **22**, 903–922 (1970)
  34. A. Ramesh Babu, S. Yusub, Ascendancy of iron ions on lithium ion conductivity, optical band gap, Urbach energy and topology of LiF–SrO–B<sub>2</sub>O<sub>3</sub> glasses. *J. Non-Cryst. Solids.* **533**, 119906 (2020)
  35. F. Urbach, The long-wavelength edge of photographic sensitivity and of the electronic absorption of solids. *Phys. Rev.* **92**, 1324 (1953)

36. R.J. Amjad, M.R. Sahar, S.K. Ghoshal, M.R. Dousti, R. Arifin, Synthesis and characterization of Dy<sup>3+</sup> doped zinc-lead-phosphate glass. *Opt. Mater.* **35**, 1103–1108 (2013)
37. S.F. Khor, Z.A. Talib, W.M. Mat Yunus, Optical properties of ternary zinc magnesium phosphate glasses. *Ceram. Int.* **38**, 935–940 (2012)
38. K.M. Kaky, M.I. Sayyed, M.H.A. Mhareb, A.H. Abdalsalam, K.A. Mahmoud, S.O. Baki, M.A. Mahdi, Physical, structural, optical and gamma radiation attenuation properties of germanate-tellurite glasses for shielding applications. *J. Non-Cryst. Solids.* **545**, 120250 (2020)
39. Y. Al-Hadeethi, M.I. Sayyed, Y.S. Rammah, Fabrication, optical, structural and gamma radiation shielding characterizations of GeO<sub>2</sub>-PbO-Al<sub>2</sub>O<sub>3</sub>-CaO glasses. *Ceram. Int.* **46**, 2055–2062 (2020)
40. F. Nawaz, R. Sahar, S.K. Ghoshal, J. Amjad, Spectral investigation of Sm<sup>3+</sup>/Yb<sup>3+</sup> co-doped sodium tellurite glass. *Chin. Opt. Lett.* **11–6**, 061605 (2013)
41. R. El-Mallawany, The optical properties of tellurite glasses. *J. Appl. Phys.* **72**, 1774–1777 (1992)
42. S. Hussain, R.J. Amjad, M. Tanveer, M. Nadeem, H. Mahmood, A. Sattar, A. Iqbal, I. Hussain, Z. Amjad, S.Z. Hussain, S.A. Siddique, M.R. Dousti, Optical investigation of Sm<sup>3+</sup> doped in phosphate glass. *Glass Phys. Chem.* **43**, 538–547 (2017)
43. M.K. Narayanan, H.D. Shashikala, Optical absorption and TEM studies of silver nanoparticle embedded BaO-CaF<sub>2</sub>-P<sub>2</sub>O<sub>5</sub> glasses. *AIP Conf. Proc.* **1731**, 1–4 (2016)
44. R. Mondal, D. Biswas, A.S. Das, R.K.N. Ningthemcha, D. Deb, S. Bhattacharya, S. Kabi, Influence of samarium content on structural, thermal, linear and non-linear optical properties of ZnO-TeO<sub>2</sub>-P<sub>2</sub>O<sub>5</sub> glasses. *Mater. Chem. Phys.* (2020). <https://doi.org/10.1016/j.matchemphys.2020.123561>
45. W.E. Mahmoud, W. Shirbeeney, A.A. Al-Ghamdi, S. Al-Heniti, Nanoparticles-doped aryl poly ether ether ketone for synthesis and characterization of Cd<sub>x</sub>Zn<sub>12x</sub>O novel application potentials. *J. Appl. Polym. Sci.* **116**, 2658–2667 (2010)
46. X.Y. Zhang, F.F. Chen, X.H. Zhang, W. Ji, Research progress of third-order optical nonlinearity of chalcogenide glasses. *Chin. Phys. B.* (2018). <https://doi.org/10.1088/1674-1056/27/8/084208>
47. H.N. Desai, J.M. Dhimmarr, B.P. Modi, Study of linear and non-linear optical parameters of zinc selenide thin film. *IJERA.* **5**, 117–122 (2015)
48. S. Stalin, D.K. Gaikwad, M.A. Samee, A. Edukondalu, S.K. Ahmmad, A.A. Joshi, R. Syed, Structural, optical features and gamma ray shielding properties of Bi<sub>2</sub>O<sub>3</sub>-TeO<sub>2</sub>-B<sub>2</sub>O<sub>3</sub>-GeO<sub>2</sub> glass system. *Ceram. Int.* **46**, 17325–17334 (2020)
49. V. Dimitrov, S. Sakka, Electronic oxide polarizability and optical basicity of simple oxides. *J. Appl. Phys.* **79**, 1736–1740 (1996)
50. H.M.M. Moawad, H. Jain, R. El-Mallawany, DC conductivity of silver vanadium tellurite glasses. *J. Phys. Chem. Solids* **70**, 224–233 (2009)
51. N. Elkhoshkhany, R. Abbas, R. El-Mallawany, A.J. Fraih, Optical properties of quaternary TeO<sub>2</sub>-ZnO-Nb<sub>2</sub>O<sub>5</sub>-Gd<sub>2</sub>O<sub>3</sub> glasses. *Ceram. Int.* **40**, 14477–14481 (2014)
52. M.I. Sayyed, A.A. Ati, M.H.A. Mhareb, K.A. Mahmoud, K.M. Kaky, S.O. Baki, M.A. Mahdi, Novel tellurite glass (60-x)TeO<sub>2</sub>-10GeO<sub>2</sub>-20ZnO-10BaO-xBi<sub>2</sub>O<sub>3</sub> for radiation shielding. *J. Alloys Compd.* **844**, 155668 (2020)
53. M.Y. Hanfi, M.I. Sayyed, E. Lacomme, I. Akkurt, K.A. Mahmoud, The influence of MgO on the radiation protection and mechanical properties of tellurite glasses. *Nucl. Eng.* (2020). <https://doi.org/10.1016/j.net.2020.12.012>
54. K.M. Kaky, M.I. Sayyed, M.H.A. Mhareb, A. Abdalsalam, K.A. Mahmoud, S.O. Baki, M.A. Mahdi, Physical, structural, optical and gamma radiation attenuation properties of germanate-tellurite glasses for shielding applications. *J. Non-Cryst. Solids* **545**, 120250 (2020)
55. Schott AG, Schott-radiation shielding glass, version May 2013. [www.schott.com/advanced\\_optics](http://www.schott.com/advanced_optics)
56. J. Tauc, *Amorphous and Liquid Semiconductors*, 1St edn. (Plenum, London, 1974).

**Publisher's Note** Springer Nature remains neutral with regard to jurisdictional claims in published maps and institutional affiliations.